

Head-to-head comparison of LNA, ^{MP}γPNA, INA and Invader probes targeting mixed-sequence double-stranded DNA

Raymond G. Emehiser, Eric Hall, Dale C. Guenther, Saswata Karmakar and Patrick J. Hrdlicka.

Department of Chemistry, University of Idaho, Moscow, ID-83844, USA

E-mail: hrdlicka@uidaho.edu

ELECTRONIC SUPPORTING INFORMATION

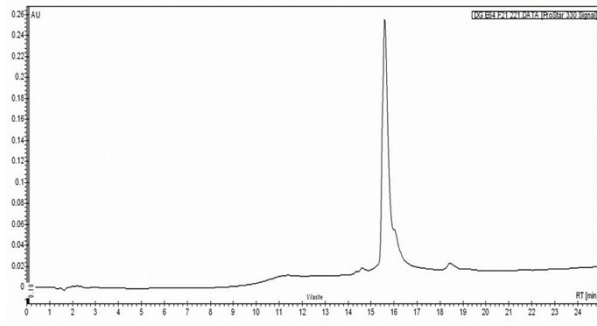
MALDI-MS of probe strands used in this study (Table S1)	S1
HPLC traces and MS spectra of probe strands used in this study (Figs. S1-S5)	S2-7
Representative thermal denaturation curves (Figs. S6 and S7)	S8-9
Preliminary characterization of Invader and INA probes	S10-24
Thermal denaturation characteristics and thermodynamics (Tables S2-S5)	S10-15
Binding to model targets (Figs. S8 and S9)	S16-18
Binding specificity (Fig. S10)	S19-20
Dose-response curves (Figs. S11 and S12; Table S6)	S21-24
Thermodynamic parameters for duplexes between LNA or ^{MP} γPNA and cDNA (Tables S7-S8)	S25-26
Additional T_m data for LNA and ^{MP} γPNA probes (Table S9)	S27
Representative electrophoretograms from dose-response studies (Fig. S13)	S28
Representative electrophoretograms from time-course studies (Fig. S14)	S29
Dose-response and time-course curves for recognition of DH1 with INV4/INA4 (Fig. S15)	S30
Sequences and T_m values of DNA hairpins used in this study (Table S10)	S31
Binding specificity of INV3 and INA3 when used at high excess (Fig. S16)	S32
Supplementary references	S33

Table S1. MALDI-MS of probe strands used in this study.^a

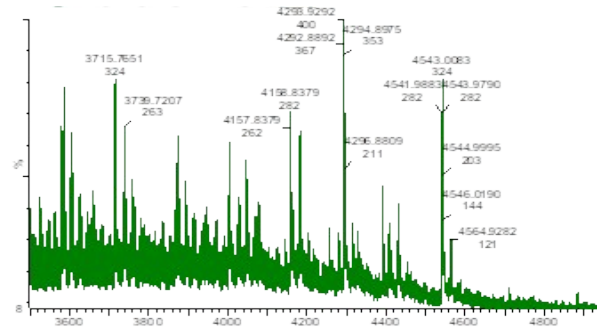
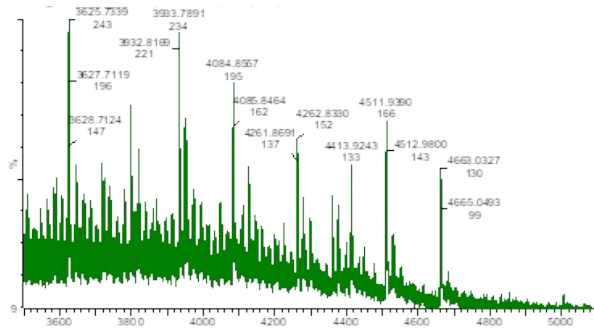
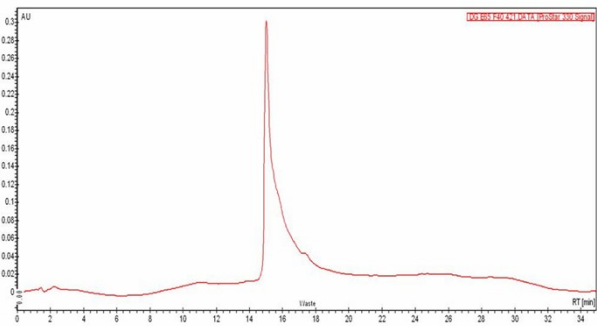
Strand	Sequence	Observed <i>m/z</i> [M+H]⁺	Calculated <i>m/z</i> [M+H]⁺
INV1 up	5'-GG <u>X</u> <u>A</u> <u>X</u> A TAT AGG C	4444	4444
INV1 down	3'-CCA <u>X</u> <u>A</u> <u>X</u> ATA TCC G	4324	4324
INV2 up	5'-GG <u>X</u> ATA T <u>A</u> <u>X</u> AGG C	4444	4444
INV2 down	3'-CCA <u>X</u> AT ATA <u>X</u> CC G	4324	4324
INV3 up	5'-GG <u>X</u> <u>A</u> <u>X</u> A T <u>A</u> <u>X</u> AGG C	4663	4661
INV3 down	3'-CCA <u>X</u> <u>A</u> <u>X</u> ATA <u>X</u> CC G	4542	4541
INV4 up	5'-GG <u>X</u> ATA <u>X</u> <u>A</u> <u>X</u> AGG C	4662	4664
INV4 down	3'-CCA <u>X</u> AT <u>A</u> <u>X</u> A <u>X</u> CC G	4542	4544
INA1 up	5'-GGT <u>I</u> AT <u>I</u> AT ATA GGC	4750	4750
INA1 down	3'-CCA <u>I</u> TA <u>I</u> TA TAT CCG	4630	4630
INA2 up	5'-GGT <u>I</u> AT ATA T <u>I</u> A GGC	4750	4750
INA2 down	3'-CCA <u>I</u> TA TAT A <u>I</u> T CCG	4630	4630
INA3 up	5'-GGT <u>I</u> AT <u>I</u> AT AT <u>I</u> AGG C	5120	5120
INA3 down	3'-CCA <u>I</u> TA <u>I</u> TA T <u>I</u> TCC G	5000	5000
INA4 up	5'-GGT <u>I</u> AT AT <u>I</u> AT <u>I</u> AGG C	5120	5120
INA4 down	3'-CCA <u>I</u> TA T <u>I</u> T <u>I</u> TCC G	5000	5000
LNA1	5'-GgT AtA TaT AgG C	4126	4126
LNA2	3'-CCa TAt Ata TCc G	4020	4020
^{MP}γPNA1	H-Lys-GGT ATA TAT AGG C-Lys-NH ₂	5389	5389
^{MP}γPNA2	NH ₂ -Lys-CCA TAT ATA TCC G-Lys-H	5269	5269
INV-T up	5'-Cy3-T <u>X</u> A-GGG-T <u>X</u> A-GGG-T <u>X</u> A-G	6184 ^b	6164
INV-T down	3'-AA <u>X</u> -CCC-AA <u>X</u> -CCC-AA <u>X</u> -C-Cy3	5909	5911
INV-T MM up	5'-Cy3-T <u>X</u> A-GCG-T <u>X</u> A-GCG-T <u>X</u> A-G	6083	6083
INV-T MM down	3'-AA <u>X</u> -CGC-AA <u>X</u> -CGC-AA <u>X</u> -C-Cy3	5991	5990

^a MALDI-MS data for **INV1/INV2 up/down** were previously reported in reference 1. ^b Presumably, the Na-adduct is observed.

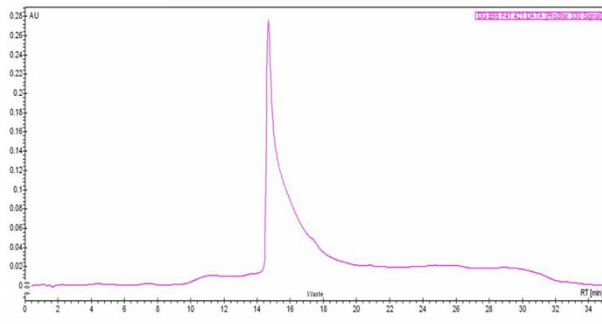
INV3up



INV3down



INV4up



INV4down

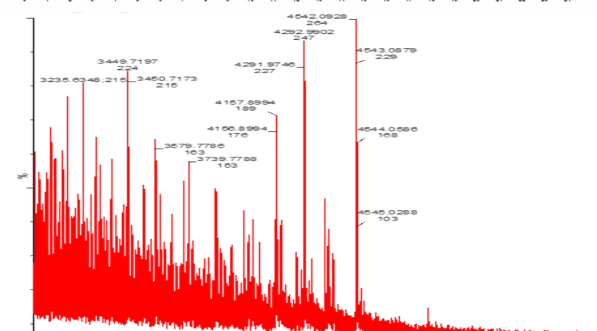
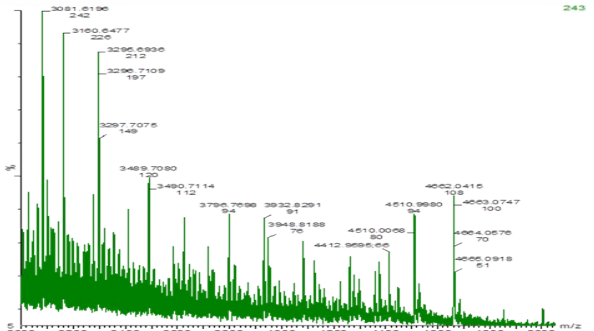
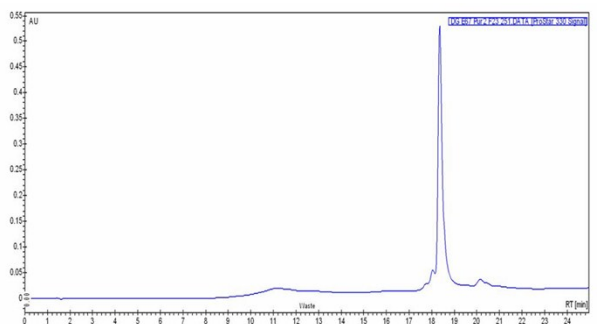
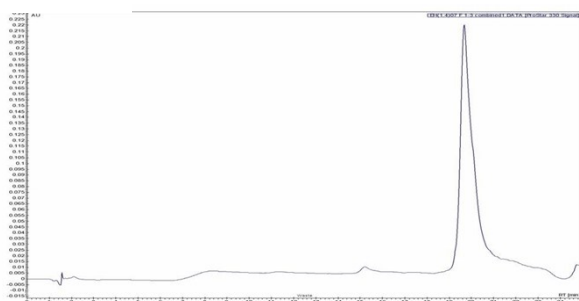
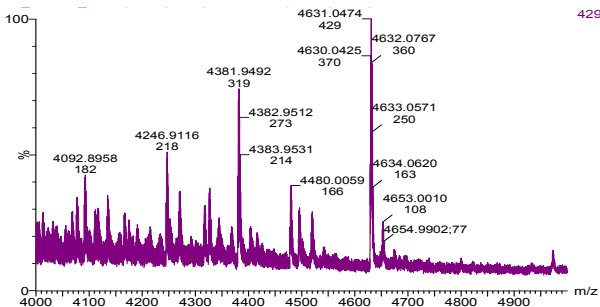
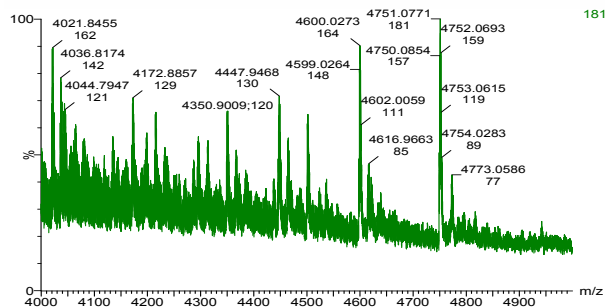
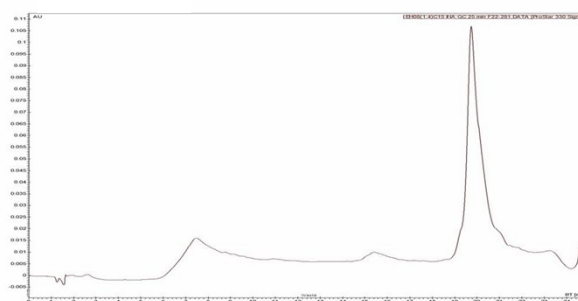


Figure S1. HPLC traces and MALDI-MS spectra for INV3/INV4 up/down.

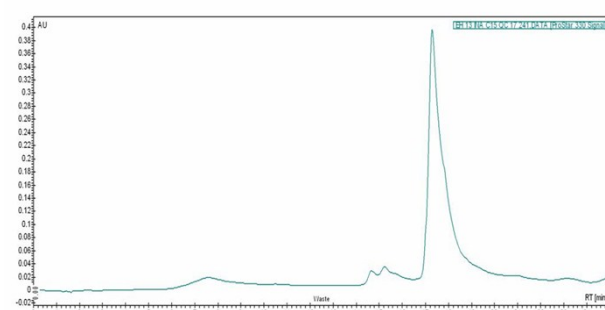
INA1up



INA1down



INA2up



INA2down

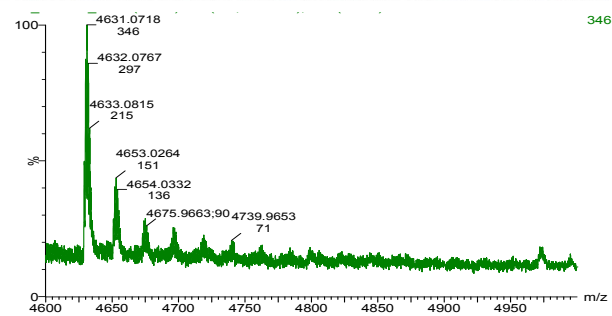
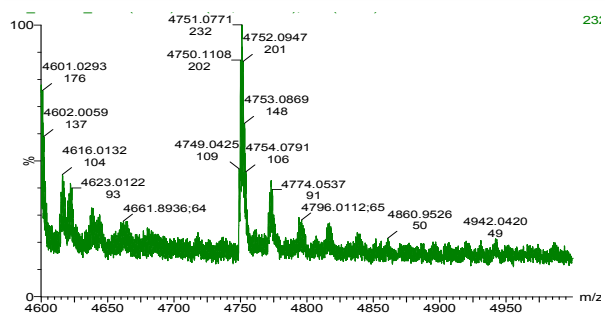
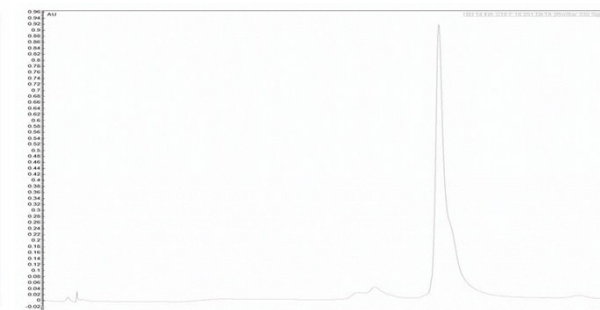


Figure S2. HPLC traces and MALDI-MS spectra for INA1/INA2 up/down.

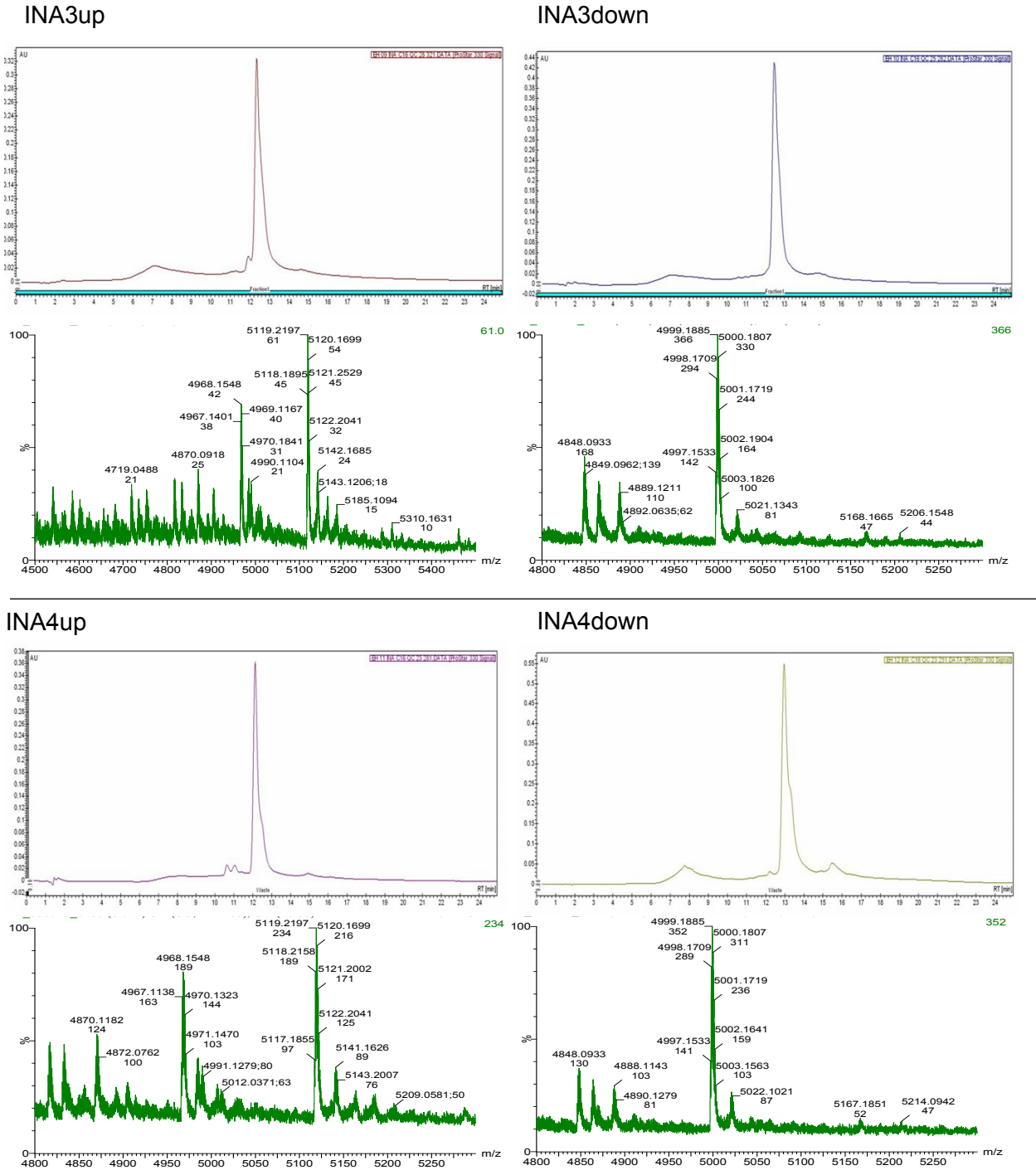
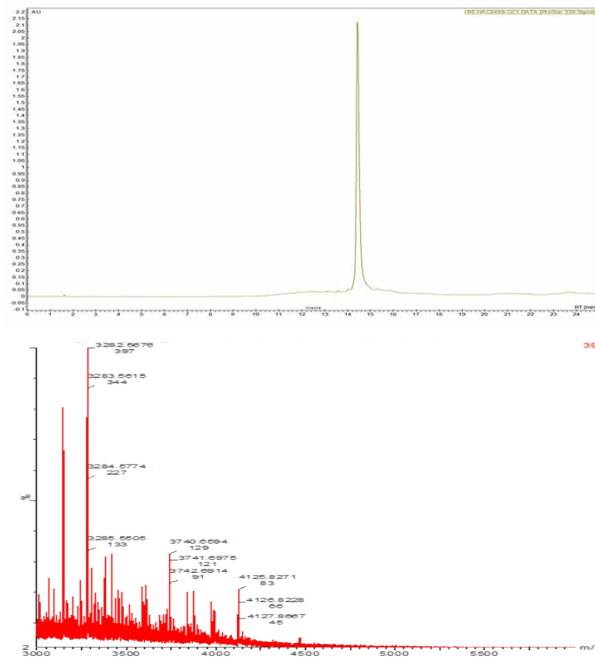
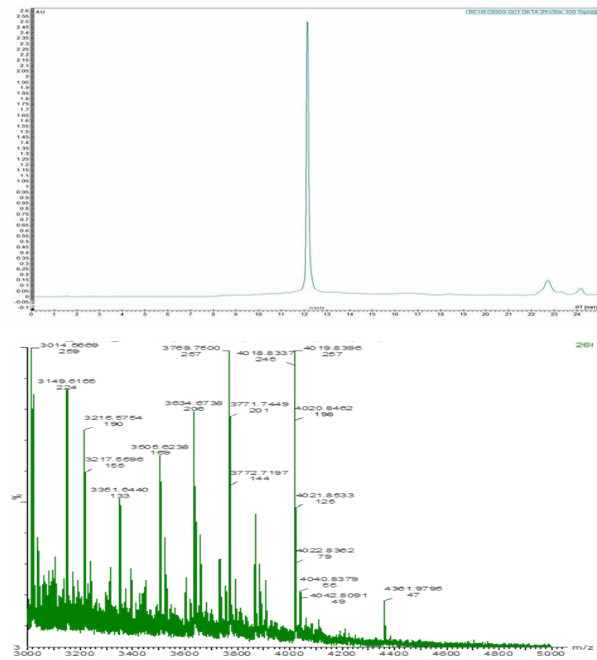


Figure S3. HPLC traces and MALDI-MS spectra for INA3/INA4 up/down.

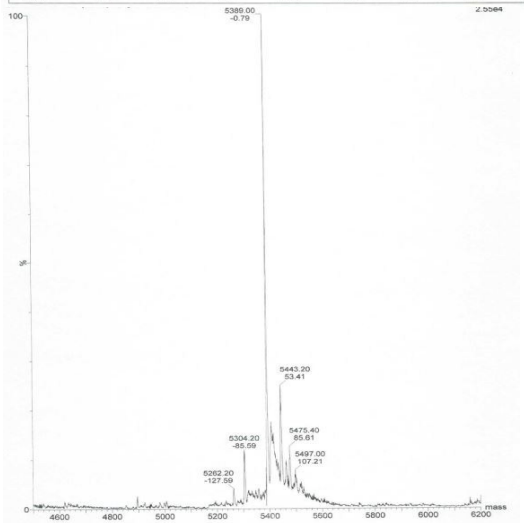
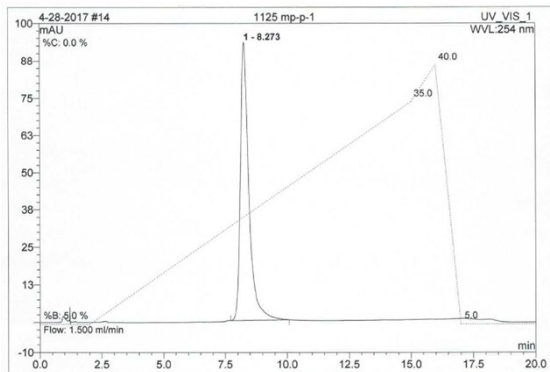
LNA1



LNA2



MP γ PNA1



MP γ PNA2

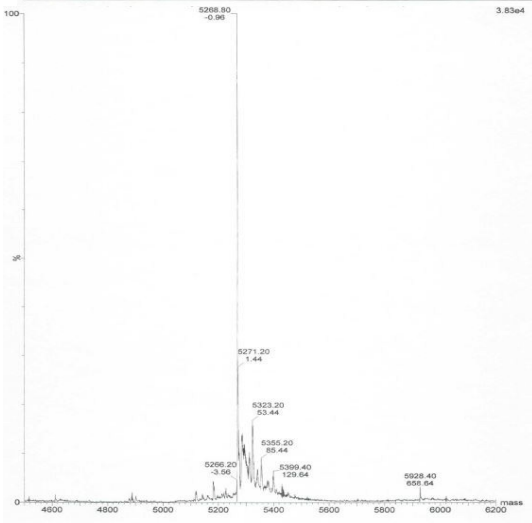
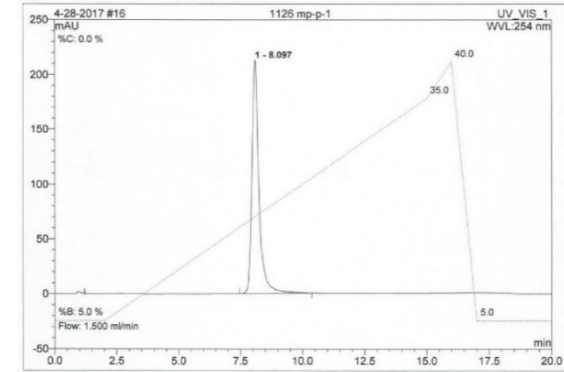


Figure S4. HPLC traces and MALDI or TOF ES+ MS spectra for LNA and MP γ PNA probes.

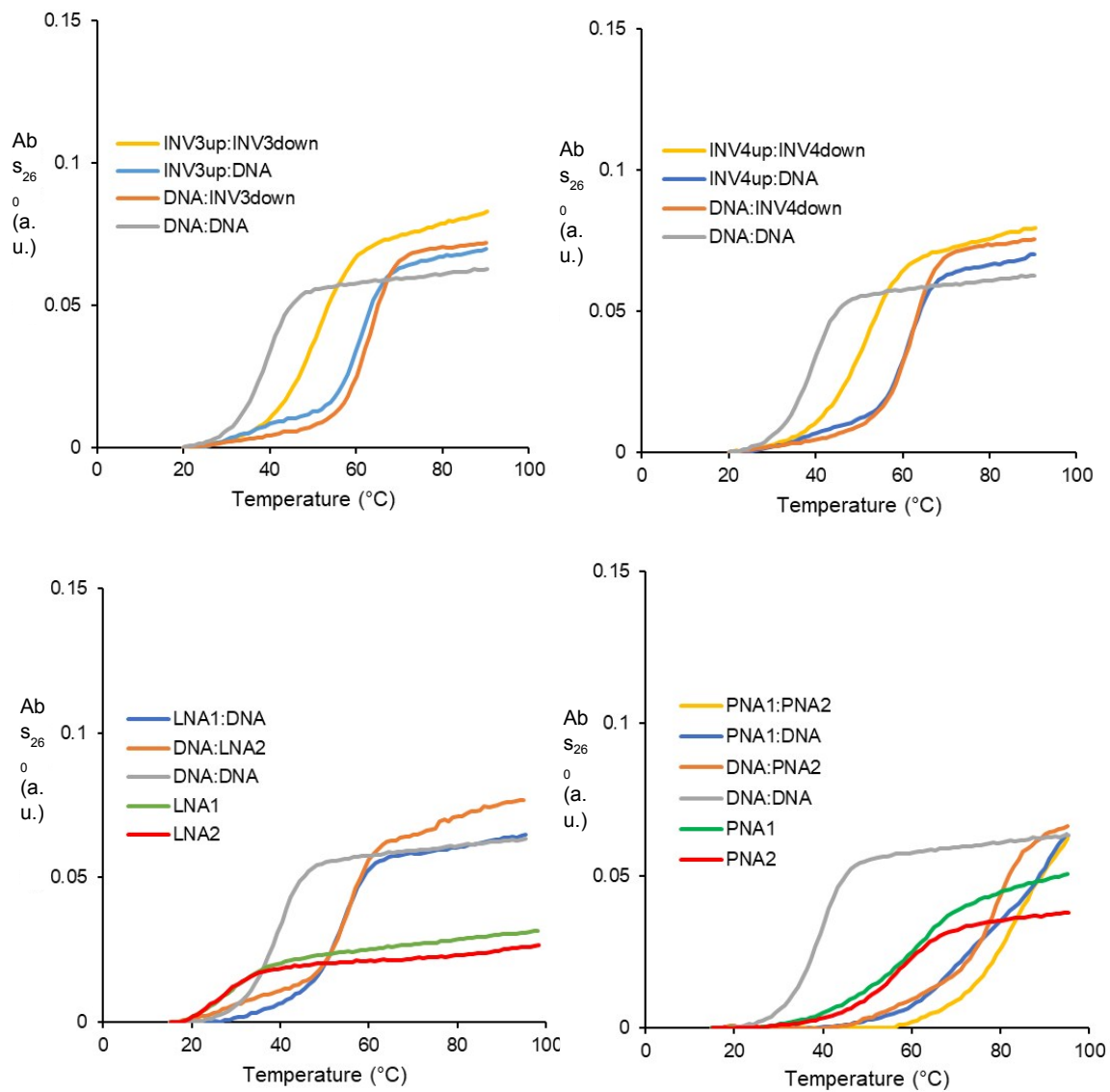


Figure S6. Representative baseline-corrected thermal denaturation curves of duplexes involving Invader, LNA and ^{MP}γPNA probes. For experimental conditions, see Table 1.

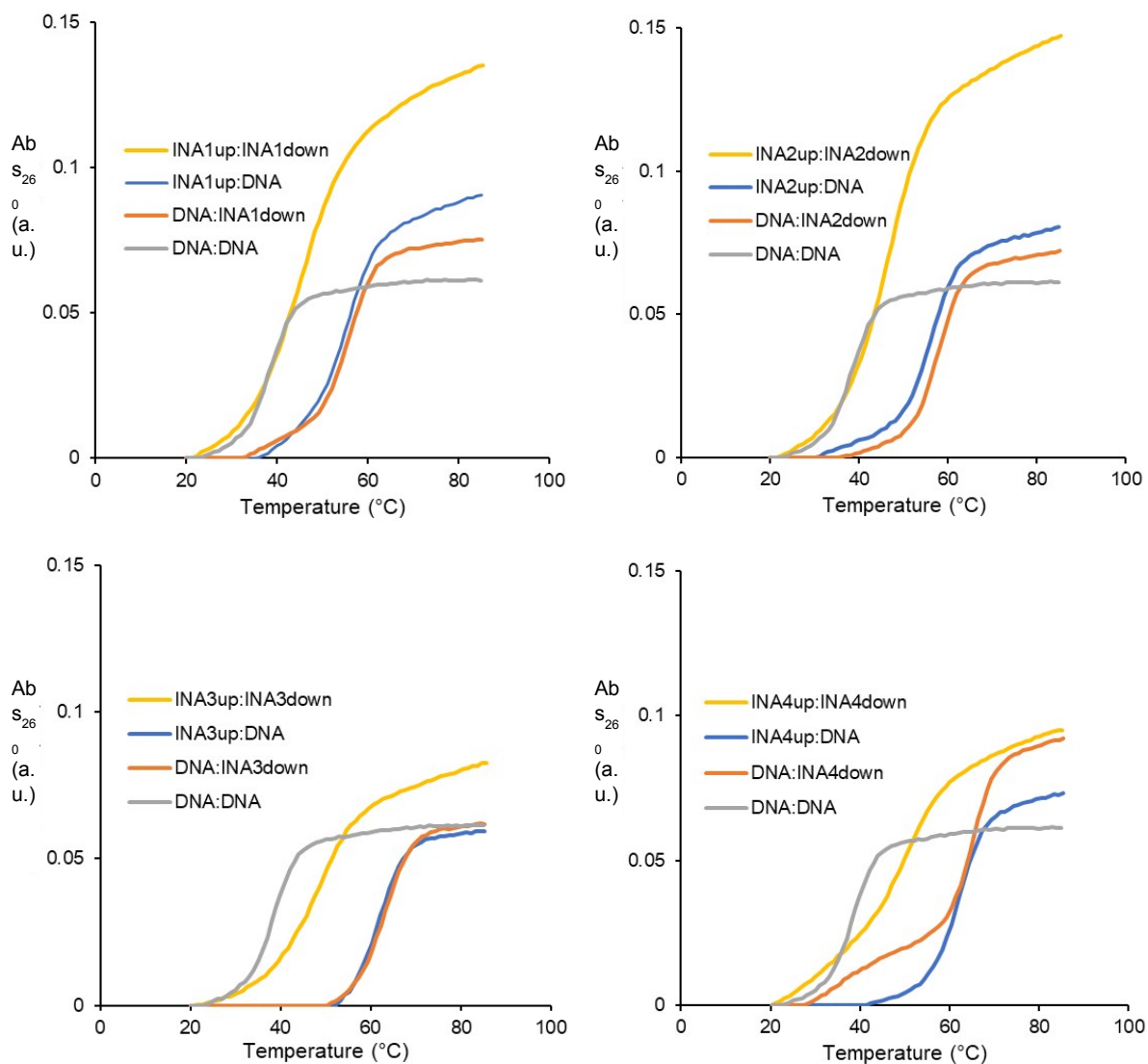


Figure S7. Representative baseline-corrected thermal denaturation curves of duplexes involving INA probes. For experimental conditions, see Table 1.

Preliminary characterization of Invader and INA probes. We have previously shown that 13-mer Invader probes with four energetic hotspots of 2'-*O*-(pyren-1-yl)methyl-RNA monomers result in very efficient recognition of model DNA hairpins but at the expense of reduced binding specificity, whereas probes with two hotspots display near-perfect binding fidelity but only moderate dsDNA-recognition.^{S1} With this in mind, we set out to evaluate Invader and INA probes with 2-3 hotspots to identify particularly promising designs (Table S2).

Thermal denaturation characteristics and thermodynamics. As expected, individual Invader strands display high affinity toward complementary DNA (cDNA), with greater absolute duplex stabilization being observed for more highly substituted strands ($\Delta T_m = 14.0\text{-}25.5$ °C, corresponding to an increase in T_m of 7.0-9.0 °C per modification, Table S2). INA strands display very similar cDNA-hybridization trends ($\Delta T_m = 16.0\text{-}25.5$ °C, Table S2). Double-stranded Invader probes denature far more readily than duplexes between individual probe strands and cDNA ($\Delta T_m = 2.5\text{-}14.5$ °C, corresponding to increases in T_m 's of 0.6-2.9 °C per modification, Table S2). Probes with two sequential energetic hotspots display particularly low T_m s (compare T_m s for **INV1** and **INV2**). Double-stranded INA probes display similar characteristics except that the modification pattern has less of an impact on T_m values ($\Delta T_m = 9.0\text{-}13.5$ °C, corresponding to increases in T_m of 2.0-2.3 °C per modification, Table S2). Invader and INA probes with three energetic hotspots display very prominent and near-identical TA values ($TA = 34.5\text{-}36.5$ °C, Table S2), whereas Invader/INA probes with two hotspots have a less pronounced driving force for dsDNA-recognition ($TA = 21.5\text{-}29.5$ °C, Table S2). **INV1**, with two sequential energetic hotspots, displays a more pronounced TA value vis-à-vis **INV2** with two separated hotspots, whereas the opposite trend is observed for the corresponding INA probes. The underlying reasons for these differences are presently not fully understood.

Table S2. Thermal denaturation temperatures of Invader and INA probe duplexes and duplexes between individual probe strands and cDNA. Also shown, are TA values for probe duplexes.^a

Probe	Sequence	T_m [ΔT_m] (°C)			TA (°C)
		probe	upper strand vs cDNA	lower strand vs cDNA	
INV1	5'-GGX AXA TAT AGG C 3'-CCA XAX ATA TCC G	40.0 [+ 2.5]	51.5 [+14.0]	55.5 [+18.0]	+29.5
INV2	5'-GGX ATA TAX AGG C 3'-CCA XAT ATA XCC G	49.0 [+11.5]	52.5 [+15.0]	55.5 [+18.0]	+21.5
INV3	5'-GGX AXA TAX AGG C 3'-CCA XAX ATA XCC G	51.0 [+13.5]	61.0 [+23.5]	63.0 [+25.5]	+35.5
INV4	5'-GGX ATA XAX AGG C 3'-CCA XAT AXA XCC G	52.0 [+14.5]	61.5 [+24.0]	62.5 [+25.0]	+34.5
INA1	5'-GGT IAT IAT ATA GGC 3'-CCA ITA ITA TAT CCG	46.5 [+ 9.0]	53.5 [+16.0]	54.5 [+17.0]	+24.0
INA2	5'-GGT IAT ATA TIA GGC 3'-CCA ITA TAT AIT CCG	47.5 [+10.0]	56.5 [+19.0]	57.5 [+20.0]	+29.0
INA3	5'-GGT IAT IAT ATI AGG C 3'-CCA ITA ITA TAI TCC G	49.5 [+12.0]	61.5 [+24.0]	61.5 [+24.0]	+36.0
INA4	5'-GGT IAT ATI ATI AGG C 3'-CCA ITA TAI TAI TCC G	51.0 [+13.5]	62.0 [+24.5]	63.0 [+25.5]	+36.5

^a Each ON was used at 1.0 μ M in T_m buffer. For experimental details, see Table 1. $TA = T_m$ (upper strand vs cDNA) + T_m (lower strand vs cDNA) - T_m (probe duplex) - T_m (dsDNA). T_m for 5'-GGTATATATAGGC:3'-CCATATATATATCCG = 37.5 °C. Data for INV1 and INV2 were previously reported in reference 1.

Thermodynamic parameters associated with duplex formation were determined by baseline fitting of thermal denaturation curves (Tables S3-S5).^{S2} Consistent with the T_m -based conclusions discussed above (Table S2), Invader and INA probes are found to be strongly thermodynamically

310

activated for dsDNA-recognition (i.e., $\Delta G^{rec} \ll 0$ kJ/mol, Table S3) due to the labile nature of the probe duplexes (i.e., $\Delta\Delta G^{310}$ between -12 and -1 kJ/mol, Table S3) relative to the highly stable nature of the probe-target duplexes (i.e., $\Delta\Delta G^{310}$ between -49 and -15 kJ/mol, Table S3). Invader and INA probes with three energetic hotspots are more strongly activated for dsDNA-recognition

310

than probes with two hotspots (e.g., $\Delta G^{rec} \sim -35$ kJ/mol for **INV1** and **INV2** vs ~ -60 kJ/mol for **INV3** and **INV4**, Table S3), because incorporation of additional intercalator-functionalized monomers has a greater stabilizing effect on probe-target duplexes than probe duplexes (e.g., compare $\Delta\Delta G^{310}$ values for duplexes involving **INV2** and **INV4**, Table S3). INA probes with two energetic hotspots are slightly more thermodynamically activated for dsDNA-recognition than the

310

corresponding Invader probes (e.g., $\Delta G^{rec} = -35$ kJ/mol and -43 kJ/mol for **INV1** and **INA1**, respectively, Table S3), whereas only minor chemistry-dependent differences are observed for triple hotspot probes.

Invader- and INA-mediated recognition of isosequential dsDNA targets is very strongly enthalpically favored (ΔH_{rec} between -386 kJ/mol and -204 kJ/mol, Table S4), which is a manifestation of enthalpically destabilized probe duplexes ($\Delta\Delta H$ between +71 kJ/mol to +168 kJ/mol, Table S4) and enthalpically stabilized duplexes between individual probe strands and cDNA ($\Delta\Delta H$ between -212 kJ/mol to -5 kJ/mol, Table S4). As discussed in the main manuscript, these trends are in line with expectations inasmuch the high intercalator density of Invader and

INA probe duplexes results in a violation of the nearest-neighbor exclusion principle^{S3,S4} and localized helix perturbation, whereas duplexes between individual probe strands and cDNA are stabilized due to strong stacking interactions between the intercalators and flanking base-pairs. The favorable change in enthalpy upon Invader- or INA-mediated recognition of isosequential

310

dsDNA is partly offset by an unfavourable decrease in entropy (i.e., $-T\Delta S^{rec} \gg 0$ kJ/mol, Table S5).

Table S3. Change in Gibbs free energy at 310 K (ΔG^{310}) upon formation of Invader/INA probe duplexes and duplexes between individual probe strands and cDNA. Also shown is the calculated change in reaction free energy upon Invader- or INA-mediated recognition of the isosequential

310

dsDNA target (ΔG^{rec}).^a

Probe	Sequence	ΔG^{310} [$\Delta\Delta G^{310}$] (kJ/mol)			310 ΔG^{rec} (kJ/mol)
		probe	upper strand vs cDNA	lower strand vs cDNA	
INV1	5'-GGX AXA TAT AGG C 3'-CCA XAX ATA TCC G	-42 [-1]	-56 [-15]	-63 [-21]	-35
INV2	5'-GGX ATA TAX AGG C 3'-CCA XAT ATA XCC G	-48 [-6]	-60 [-18]	-65 [-23]	-35
INV3	5'-GGX AXA TAX AGG C 3'-CCA XAX ATA XCC G	-53 [-11]	-78 [-36]	-78 [-37]	-62
INV4	5'-GGX ATA XAX AGG C 3'-CCA XAT AXA XCC G	-53 [-12]	-80 [-38]	-76 [-34]	-60
INA1	5'GGT IAT IAT ATA GGC 3'-CCA ITA ITA TAT CCG	-45 [-3]	-62 [-20]	-68 [-27]	-43
INA2	5'-GGT IAT ATA TIA GGC 3'-CCA ITA TAT AIT CCG	-48 [-6]	-69 [-28]	-73 [-31]	-52
INA3	5'-GGT IAT IAT ATI AGG C 3'-CCA ITA ITA TAI TCC G	-49 [-7]	-71 [-29]	-75 [-34]	-56
INA4	5'-GGT IAT ATI ATI AGG C	-54 [-12]	-77 [-36]	-91 [-49]	-73

3'-CCA **I**TA **T**A**I** **T**A**I** TCC G

^a $\Delta\Delta G^{310}$ is determined relative to the corresponding unmodified DNA duplex ($\Delta G^{310} = -42$ 310

kJ/mol). $\Delta G^{rec} = \Delta G^{310}$ (upper probe vs cDNA) + ΔG^{310} (lower probe vs cDNA) - ΔG^{310} (probe) - ΔG^{310} (dsDNA).

Table S4. Change in enthalpy (ΔH) upon formation of Invader/INA probe duplexes and duplexes between individual probe strands and cDNA. Also shown is the calculated change in reaction enthalpy upon Invader- or INA-mediated recognition of the isosequential dsDNA target (ΔH_{rec}).^a

Probe	Sequence	ΔH [$\Delta\Delta H$] (kJ/mol)			ΔH_{rec} (kJ/mol)
		probe	upper strand vs cDNA	lower strand vs cDNA	
INV1	5'-GG X A X A TAT AGG C 3'-CCA X A X ATA TCC G	- 257 [+168]	-443 [-17]	-486 [-61]	-246
INV2	5'-GG X ATA T X AGG C 3'-CCA X AT ATA X CC G	-306 [+120]	-473 [-48]	-509 [-83]	-250
INV3	5'-GG X A X A T X AGG C 3'-CCA X A X ATA X CC G	-344 [+81]	-550 [-124]	-541 [-115]	-321
INV4	5'-GG X ATA X A X AGG C 3'-CCA X AT A X A X CC G	- 352 [+73]	-569 [-143]	-508 [-82]	-299
INA1	5'GGT I AT I AT ATA GGC 3'-CCA I TA I TA TAT CCG	-264 [+161]	-430 [-5]	-518 [-92]	-258
INA2	5'-GGT I AT ATA T I A GGC 3'-CCA I TA TAT A I T CCG	-335 [+91]	-536 [-110]	-557 [-131]	-332
INA3	5'-GGT I AT I AT AT I AGG C 3'-CCA I TA I TA T A I TCC G	- 325 [+100]	-460 [-35]	-495 [-69]	-204
INA4	5'-GGT I AT AT I AT I AGG C 3'-CCA I TA T A I T A I TCC G	-354 [+71]	-528 [-103]	-637 [-212]	-386

^a $\Delta\Delta H$ is determined relative to the corresponding unmodified DNA duplex ($\Delta H = -426$ kJ/mol).
 $\Delta H_{rec} = \Delta H$ (upper probe vs cDNA) + ΔH (lower probe vs cDNA) - ΔH (probe) - ΔH (dsDNA).

Table S5. Change in entropy at 310 K ($-T\Delta S^{310}$) upon formation of Invader/INA probe duplexes and duplexes between individual probe strands and cDNA. Also shown is the calculated change in reaction entropy at 310 K upon Invader- or INA-mediated recognition of the isosequential dsDNA target ($-T\Delta S^{rec}$).^a

Probe	Sequence	$-T\Delta S^{310}$ [$\Delta(T\Delta S^{310})$] (kJ/mol)			$-T\Delta S^{310}$ <i>rec</i> (kJ/mol)
		probe	upper strand vs cDNA	lower strand vs cDNA	
INV1	5'-GGX AXA TAT AGG C 3'-CCA XAX ATA TCC G	217 [-167]	395 [+11]	423 [+39]	+217
INV2	5'-GGX ATA TAX AGG C 3'-CCA XAT ATA XCC G	257 [-126]	413 [+30]	444 [+60]	+216
INV3	5'-GGX AXA TAX AGG C 3'-CCA XAX ATA XCC G	292 [-92]	472 [+88]	462 [+79]	+258
INV4	5'-GGX ATA XAX AGG C 3'-CCA XAT AXA XCC G	299 [-85]	489 [+105]	432 [+49]	+239
INA1	5'-GGT IAT IAT ATA GGC 3'-CCA ITA ITA TAT CCG	219 [-164]	368 [-15]	449 [+66]	+215
INA2	5'-GGT IAT ATA TIA GGC 3'-CCA ITA TAT AIT CCG	286 [-97]	466 [+83]	483 [+100]	+280
INA3	5'-GGT IAT IAT ATI AGG C 3'-CCA ITA ITA TAI TCC G	276 [-108]	389 [+6]	419 [+35]	+148
INA4	5'-GGT IAT ATI ATI AGG C 3'-CCA ITA TAI TAI TCC G	300 [-84]	450 [+67]	546 [+162]	+313

^a $\Delta(T\Delta S^{310})$ is measured relative to the corresponding unmodified DNA duplex ($-T\Delta S^{310} = 384$ kJ/mol).

$-T\Delta S^{rec} = \Delta(T^{310}\Delta S)$ (upper probe vs cDNA) + $\Delta(T^{310}\Delta S)$ (lower probe vs cDNA) - $\Delta(T^{310}\Delta S)$ (probe).

Binding to model targets. Model target **DH1** was incubated with a 5-fold molar excess of Invader or INA probes at 37 °C (for a description of the assay, please refer to the main manuscript and

310

Figure 2). As anticipated from the prominent TA and ΔG^{rec} values (Tables S2 and S3, respectively), all Invader and INA probes recognize **DH1** to some degree (Figure S8). Invader probes with three energetic hotspots recognize **DH1** more efficiently than probes with two hotspots (~75% vs 20-35%, respectively, Figure S8). Similar trends are observed for INA probes, with triple hotspot INAs displaying comparable levels of **DH1**-recognition vis-à-vis the corresponding Invader probes (65-75%). Dual hotspot INA probes recognize **DH1** more efficiently than the corresponding Invader probes (45-60% vs. 25-30%).

Room temperature incubation of 100-fold molar excess of Invader or INA probes with **DH1** - i.e., conditions at which the probes ($T_m = 40-52$ °C, Table S2) and **DH1** ($T_m = 58.5$ °C, Table S10) display minimal denaturation - also results in recognition of the double-stranded stem regions (53%, 57%, 92%, 72% for probe **INV1-INV4** and 49%, 53% 66%, 75% for probes **INA1-INA4** respectively Figure S9). As expected, **DH1** recognition is less efficient at room temperature than at 37 °C, since it is more difficult to overcome the activation barriers for **DH1**-recognition (i.e., partial probe or target denaturation).

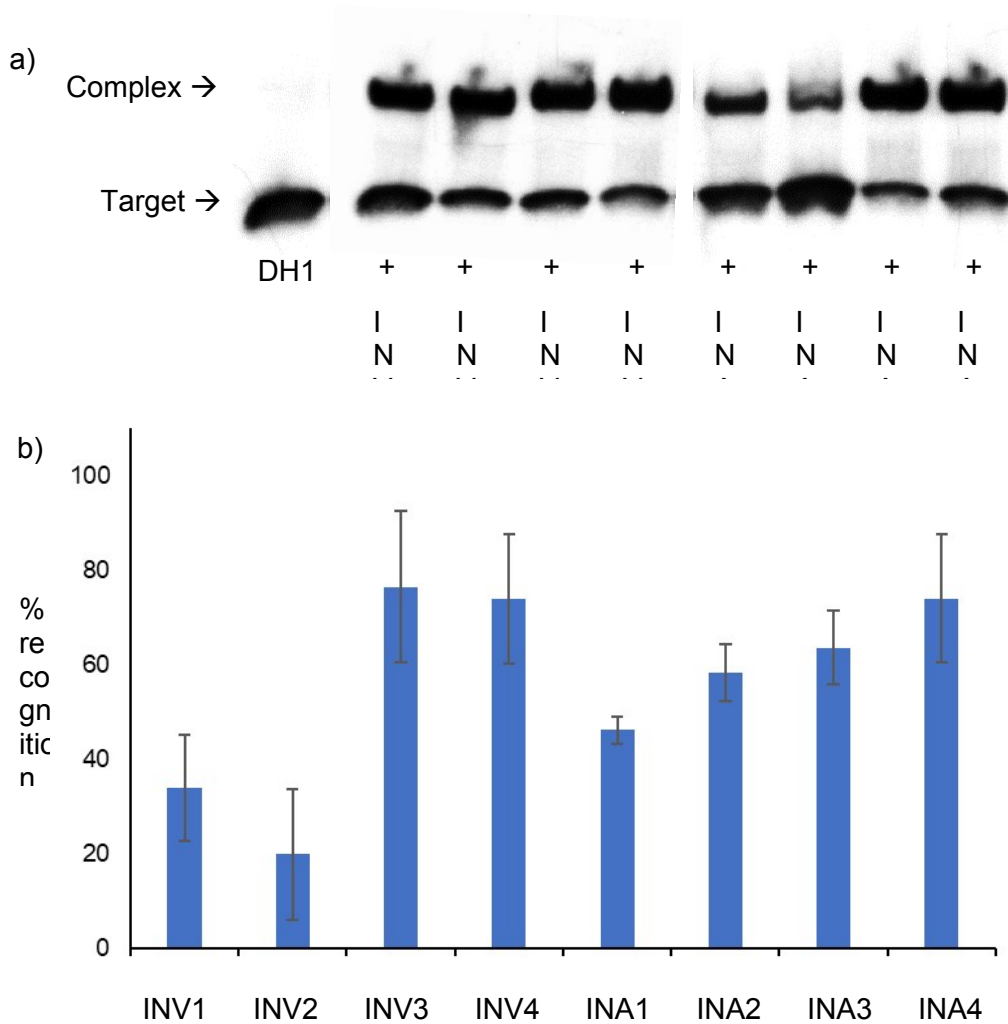


Figure S8. A) Representative electrophoretograms for recognition of model dsDNA target **DH1** (34.4 nM) using a 5-fold molar excess of various Invader and INA probes at 37 °C. B) Histograms depict averaged results from at least three separate experiments; error bars represent standard deviation. DIG-labeled **DH1** (5'-GGTATATATAGGC-T₁₀-GCCTATATATACC-3') was incubated with the specified pre-annealed Invader or INA probes in HEPES buffer (50 mM HEPES, 100 mM NaCl, 5 mM MgCl₂, pH 7.2, 10% sucrose, 1.44 mM spermine tetrahydrochloride) at 37 °C for 2.5 h.

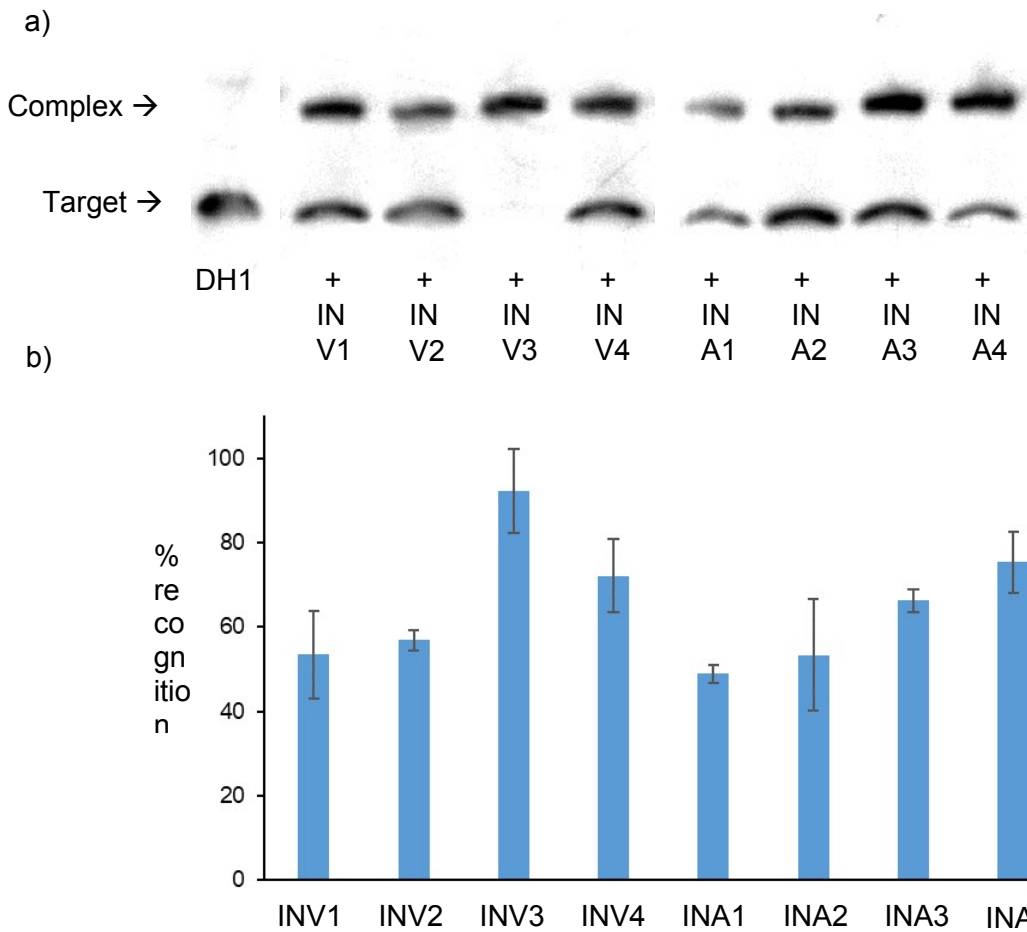


Figure S9. A) Representative electrophoretograms for recognition of model dsDNA target **DH1** (34.4 nM) using a 100-fold molar excess of various Invader and INA probes at room temperature. B) Histograms depict averaged results from at least three separate experiments; error bars represent standard deviation. DIG-labeled **DH1** was incubated with the specified pre-annealed Invader or INA probes in HEPES buffer at room temperature for 17 h. For other experimental details, see Figure S8.

Binding specificity. A preliminary evaluation of binding specificity for the eight Invader and INA probes was performed using DNA hairpin **DH2**, which has a stem region that differs in sequence at one position relative to the probes (italicized residues indicate positions of sequence deviation, Figure S10). Excellent binding specificity is generally observed when incubating a 5-fold excess of the Invader and INA probes with **DH2** at 37 °C (Figure S10 – panel a). Conversely, significant binding (20-40%) is observed for probes with three energetic hotspots when incubated at 100-fold excess with **DH2** at room temperature (Figure S10 – panels b and c). The greater binding specificity at 37 °C vis-à-vis room temperature likely reflects the decreased stability of mismatched probe-target complexes at higher experimental temperatures.

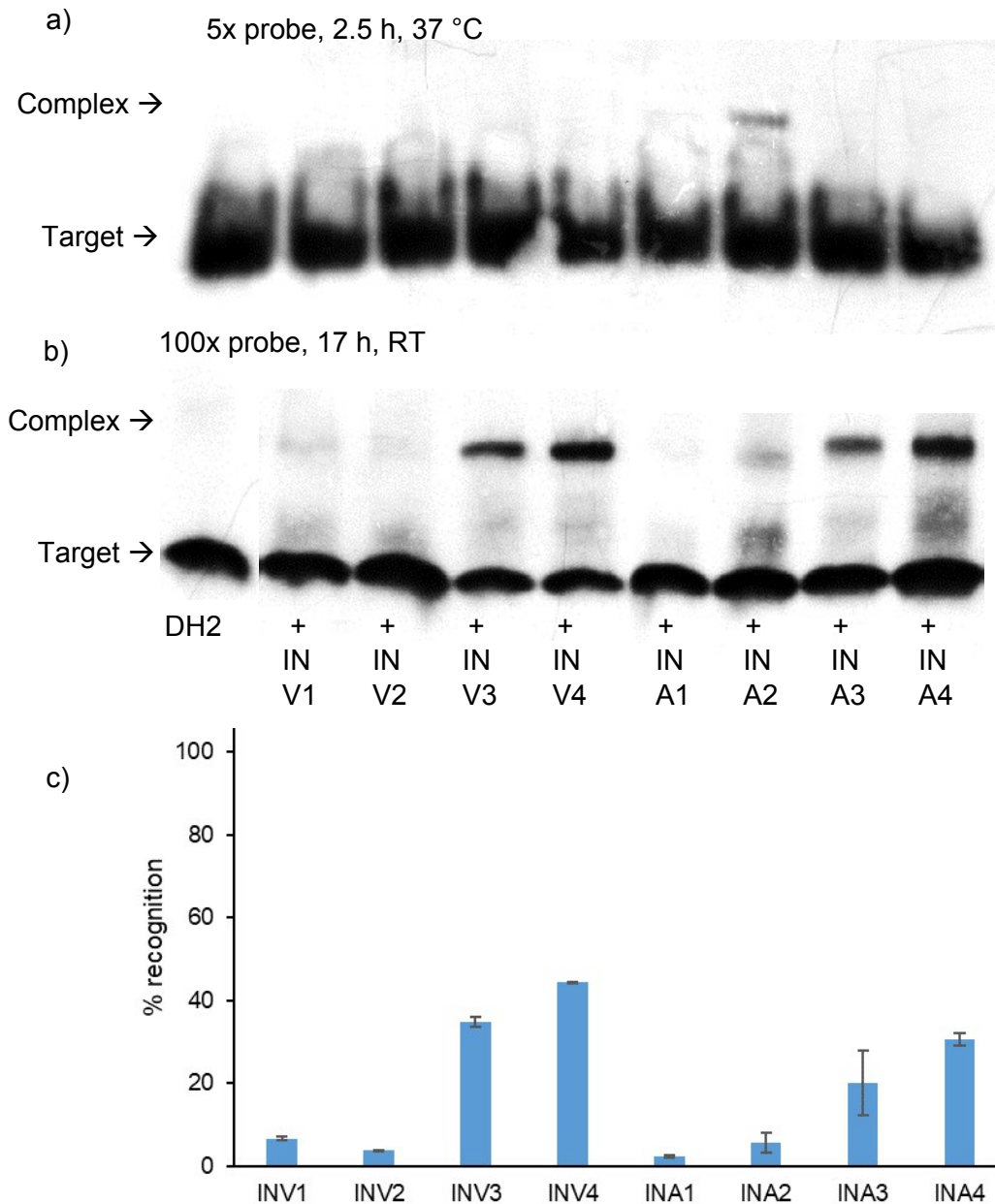


Figure S10. Representative electrophoretograms for recognition of DNA hairpin **DH2** (34.4 nM) - featuring a fully base-paired stem region that differs in sequence at one position vis-à-vis Invader and INA probes - using A) a 5-fold probe excess at 37 °C or B) a 100-fold probe excess at room temperature. C) Histograms depict averaged results from at least three separate recognition experiments (100-fold excess, room temperature); error bars represent standard deviation. **DH2:** 5'-GGTATTTATAGGC-T₁₀-GCCTATAAATACC-3'). For incubation conditions, see Figure S8.

Dose-response curves. Based on the observed TA and ΔG^{rec} trends (Tables S2 and S3, respectively) and preliminary results from the electrophoretic mobility shift assays (Figures S8-S10), we chose to study Invader and INA probes with three energetic hotspots in greater detail (see below) and compare them to corresponding LNA and $^{MP}\gamma$ PNA probes (see main manuscript). Dose-response curves were obtained allowing for determination of C_{50} values at room temperature (Figures S11 and S12) and 37 °C (Figure 5 in the main manuscript). Considerably lower C_{50} values were observed at 37 °C since partial probe denaturation is facilitated and base-pairing in the target is more dynamic. Triple hotspot Invader and INA probes recognize the targets with similar efficiency ($C_{50,RT} = 0.7-1.8 \mu\text{M}$; $C_{50,37^\circ\text{C}} = 31-48 \text{ nM}$, Table S6).

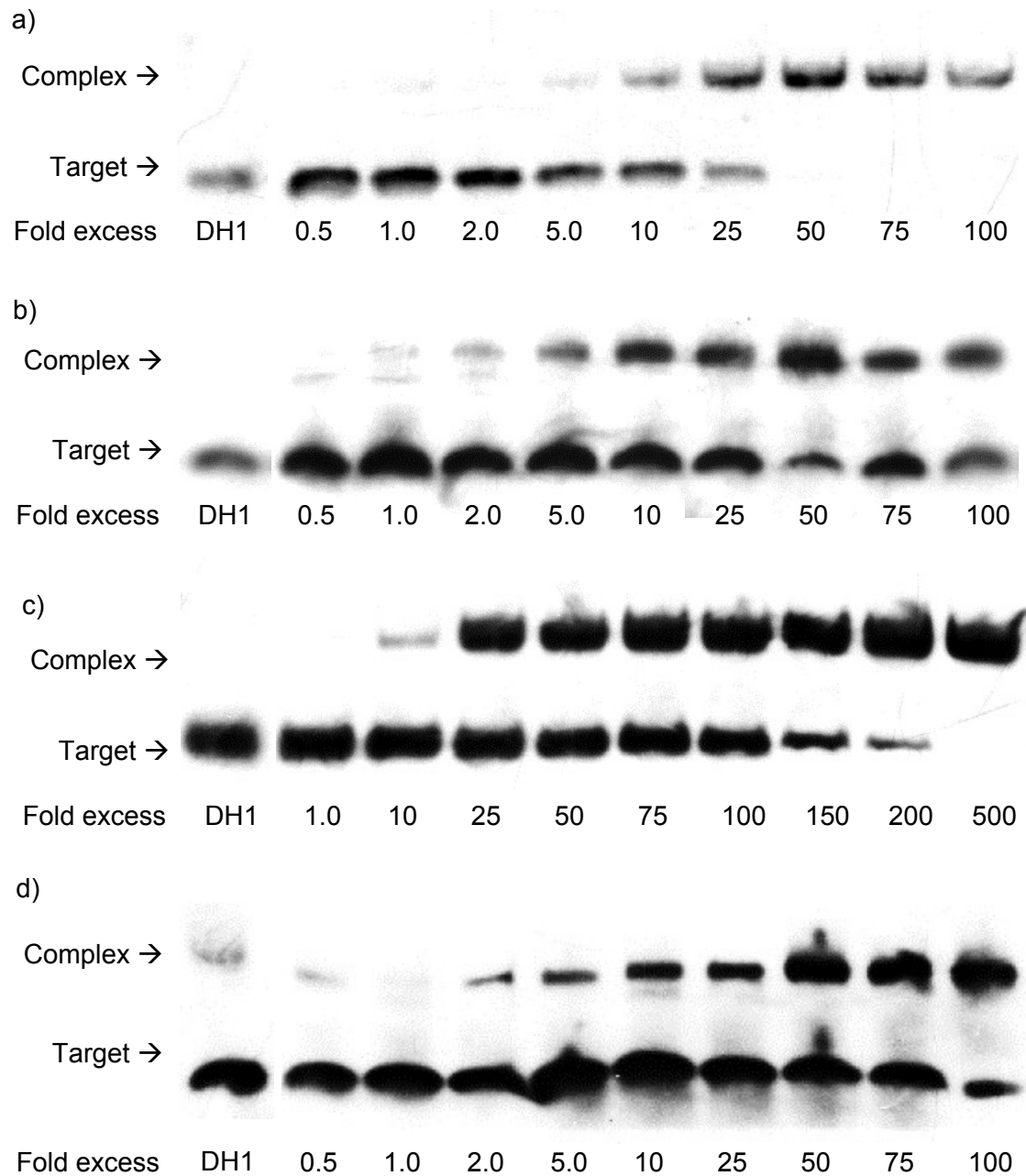


Figure S11. Representative electrophoretograms for recognition of **DH1** (34.4 nM) using different concentrations of a) **INV3**, b) **INV4**, c) **INA3**, or d) **INA4**. Probes were incubated with **DH1** in HEPES buffer at room temperature for 17 h. For additional experimental details, see Figure S8.

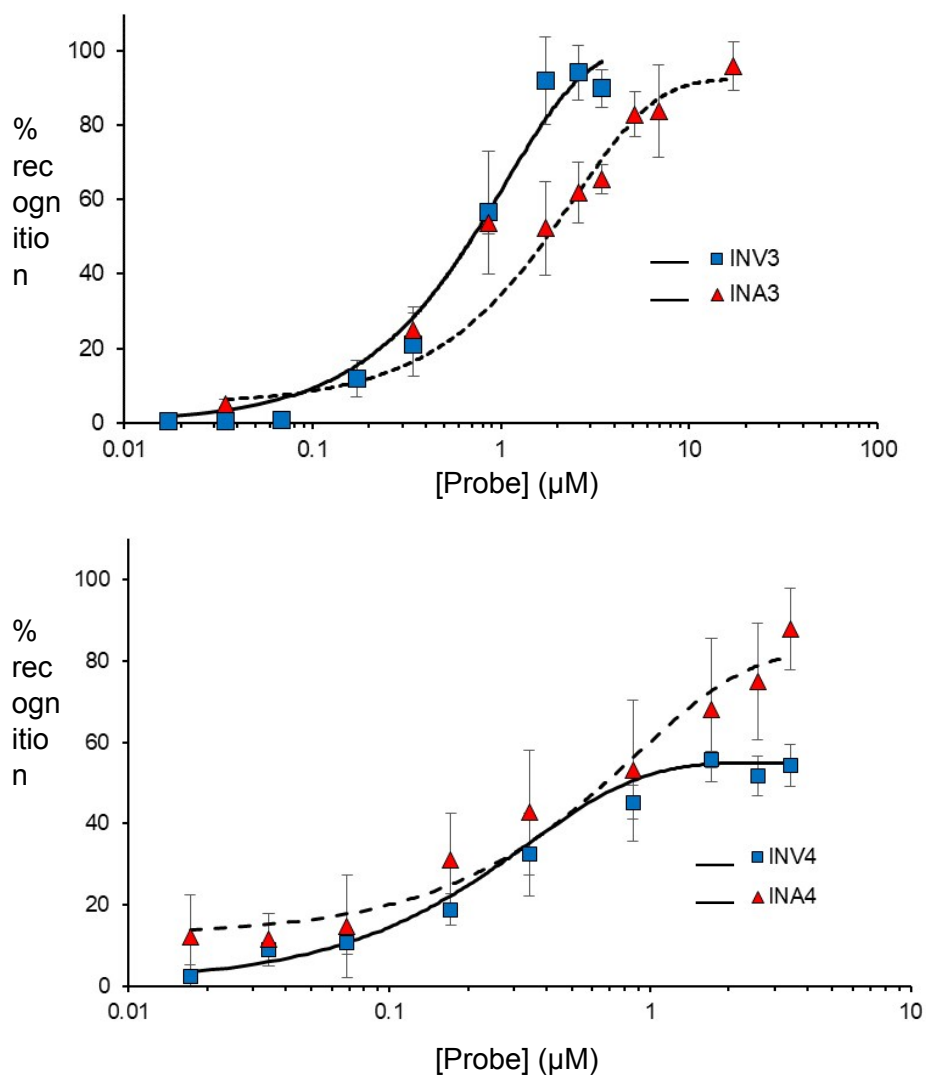


Figure S12. Dose-response curves for Invader and INA probes with three energetic hotspots. Probes were incubated with **DH1** (34.4 nM) at room temperature for 17 h. Curves represent averages of at least three independent experiments. For additional details regarding experimental conditions, see Figure S8.

Table S6. C_{50} values for recognition of **DH1** using Invader and INA probes with three energetic hotspots at room temperature (RT) or 37° C. Please note the difference in the concentration scale at the two different temperatures.^a

Probe	C_{50} RT (μM)	C_{50} 37 °C (nM)
INV3	0.7	48
INV4	0.8	44
INA3	1.8	41
INA4	0.7	31

^a C_{50} values, i.e., probe concentrations resulting in 50% target recognition, are calculated from Figures 5, S12 and S15.

Thermodynamic parameters for duplexes between LNA or ^{MP}γPNA and cDNA. As expected from the observed T_m trends (Table 1), duplex formation between LNA or ^{MP}γPNA probes and cDNA is associated with strongly negative - and thus favorable - $\Delta\Delta G^{310}$ values (Table 2). Comparison of $\Delta\Delta G^{310}$ values suggests that the cDNA affinity of individual probe strands follows the order: ^{MP}γPNA >> Invader ~ INA > LNA (Table 2 and Tables S3). The stabilization of LNA:cDNA and ^{MP}γPNA:cDNA duplexes is a consequence of favorable enthalpic factors (Table S7) that are partly offset by unfavorable decreases in entropy (Table S8).

310

Comparison of the calculated ΔG^{rec} values for dsDNA-recognition using Invader or INA probes with three hotspots (Table S3) and $\Delta\Delta G^{310}$ values for LNA:cDNA and ^{MP}γPNA:cDNA

310

duplexes (Table 2; $\Delta G^{rec} = \Delta\Delta G^{310}$ for single-stranded probes), suggests that the available thermodynamic driving force for dsDNA-recognition is similar for ^{MP}γPNA and optimized INA and Invader probes, whereas dsDNA-recognition is thermodynamically less favorable with LNA

310

probes. However, the ΔG^{rec} values for LNA and ^{MP}γPNA probes are likely less favorable due to a proclivity for dimerization (Table S9). Melting of these secondary structures must be overcome during the dsDNA-recognition process. Similar conclusions are reached upon comparison of TA values for Invader or INA probes with three hotspots (Table S2) and ΔT_m values for LNA:cDNA and ^{MP}γPNA:cDNA duplexes (Table 1; $TA = \Delta T_m$ for single-stranded probes).

Table S7. Change in enthalpy (ΔH) upon formation of duplexes between individual LNA or ^{MP} γ PNA strands and cDNA.^a

Probe	Sequence	ΔH [$\Delta\Delta H$] (kJ/mol)
LNA1	5'-GgT AtA TAt AgG C	- 491 [-66]
LNA2	3'-CCa Tat Ata TCc G	-535 [-110]
^{MP} γ PNA1	H-Lys-GGT ATA TAT AGG C-Lys-NH ₂	nd
^{MP} γ PNA2	NH ₂ -Lys-CCA TAT ATA TCC G-Lys-H	-593 [-167]

^a $\Delta\Delta H$ is determined relative to the corresponding unmodified DNA duplex ($\Delta H = -426$ kJ/mol). nd = not determined due to unclear upper baseline.

Table S8. Change in entropy at 310 K ($-T\Delta S^{310}$) upon formation of duplexes between individual LNA or ^{MP} γ PNA strands and cDNA.^a

Probe	Sequence	$-T\Delta S^{310}$ [$\Delta(T\Delta S^{310})$] (kJ/mol)
LNA1	5'-GgT AtA TAt AgG C	428 [+44]
LNA2	3'-CCa Tat Ata TCc G	468 [+84]
^{MP} γ PNA1	H-Lys-GGT ATA TAT AGG C-Lys-NH ₂	nd
^{MP} γ PNA2	NH ₂ -Lys-CCA TAT ATA TCC G-Lys-H	484 [+100]

^a $\Delta(T\Delta S^{310})$ is measured relative to the corresponding unmodified DNA duplex ($-T\Delta S^{310} = 384$ kJ/mol). nd = not determined due to unclear upper baseline.

Table S9. Thermal denaturation experiments exploring the nature of secondary structures formed by LNA and ^{MP}γPNA probes in absence of cDNA. The higher T_m s observed when using higher probe concentrations suggest that the secondary structures involve duplex formation (dimerization, intermolecular recognition) rather than hairpin formation (intramolecular recognition). Also shown is the change in Gibbs free energy at 310 K (ΔG^{310}) upon probe dimerization.^a

Probe	Sequence	T_m (°C)		ΔG^{310} [$\Delta\Delta G^{310}$] (kJ/mol)
		[probe] = 1 μ M	[probe] = 10 μ M	[probe] = 1 μ M
LNA1	5'-GgT AtA TaT AgG C	29.0	33.0	nd
LNA2	3'-CCa TAt Ata TCc G	27.0	31.0	nd
^{MP} γPNA1	H-Lys-GGT ATA TAT AGG C-Lys-NH ₂	62.0	67.5	-53 [-11]
^{MP} γPNA2	H-Lys-GCC TAT ATA TAC C-Lys-NH ₂	57.5	65.0	-54 [-12]

^a Only one 10 μ M experiment was performed to conserve probes. For experimental conditions, see Table 1 in the main manuscript. $\Delta\Delta G^{310}$ calculated relative to the corresponding unmodified DNA duplex ($\Delta G^{310} = -42$ kJ/mol). nd = not determined due to unclear baseline.

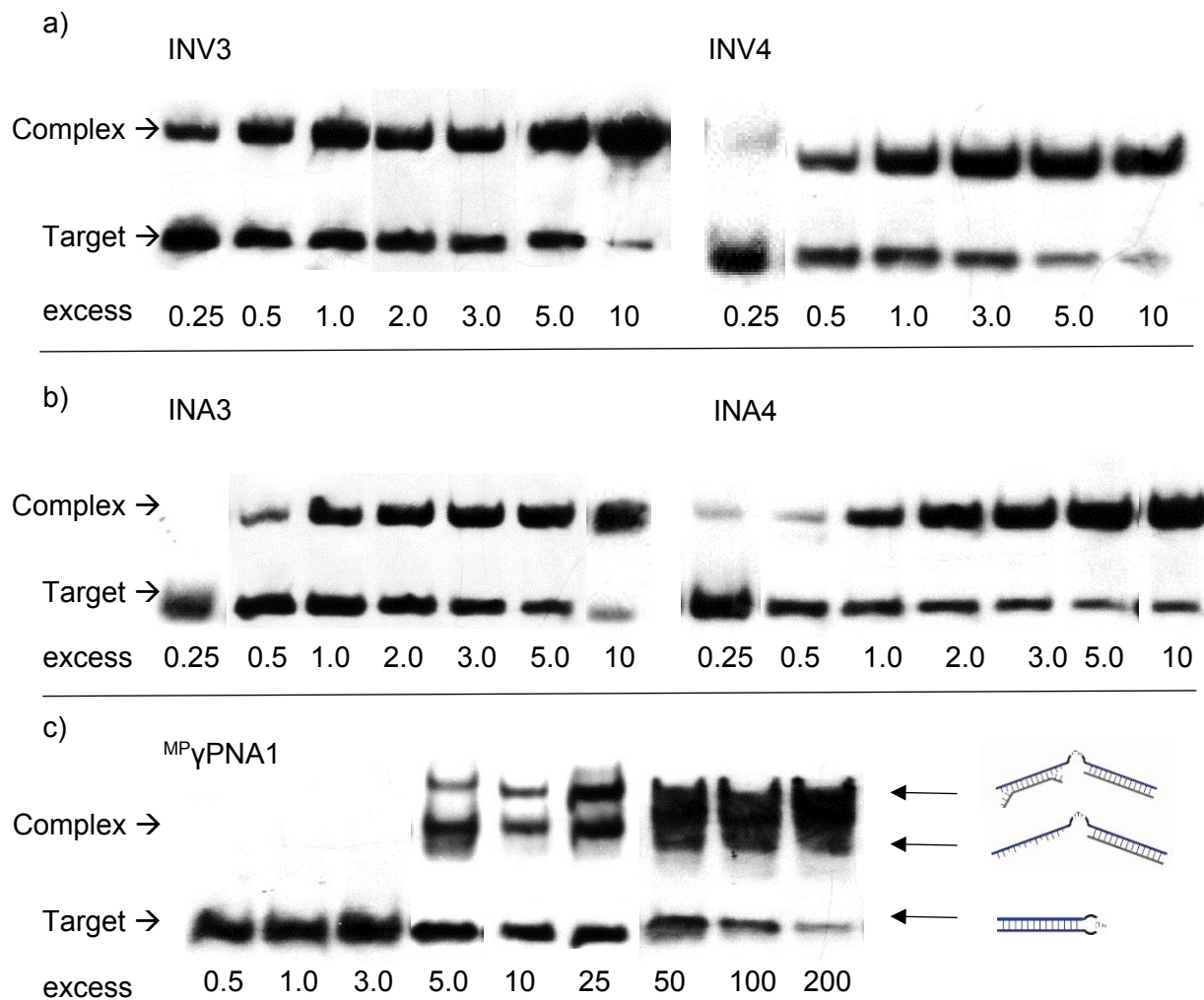


Figure S13. Representative electrophoretograms for recognition of model dsDNA target **DH1** (34.4 nM) using different concentrations of Invader, INA and ^{MP} γ PNA probes at 37 °C for 2.5 hours. For additional details regarding experimental conditions, see Figure S8. For dose-response curves, see Figures 5 and S15.

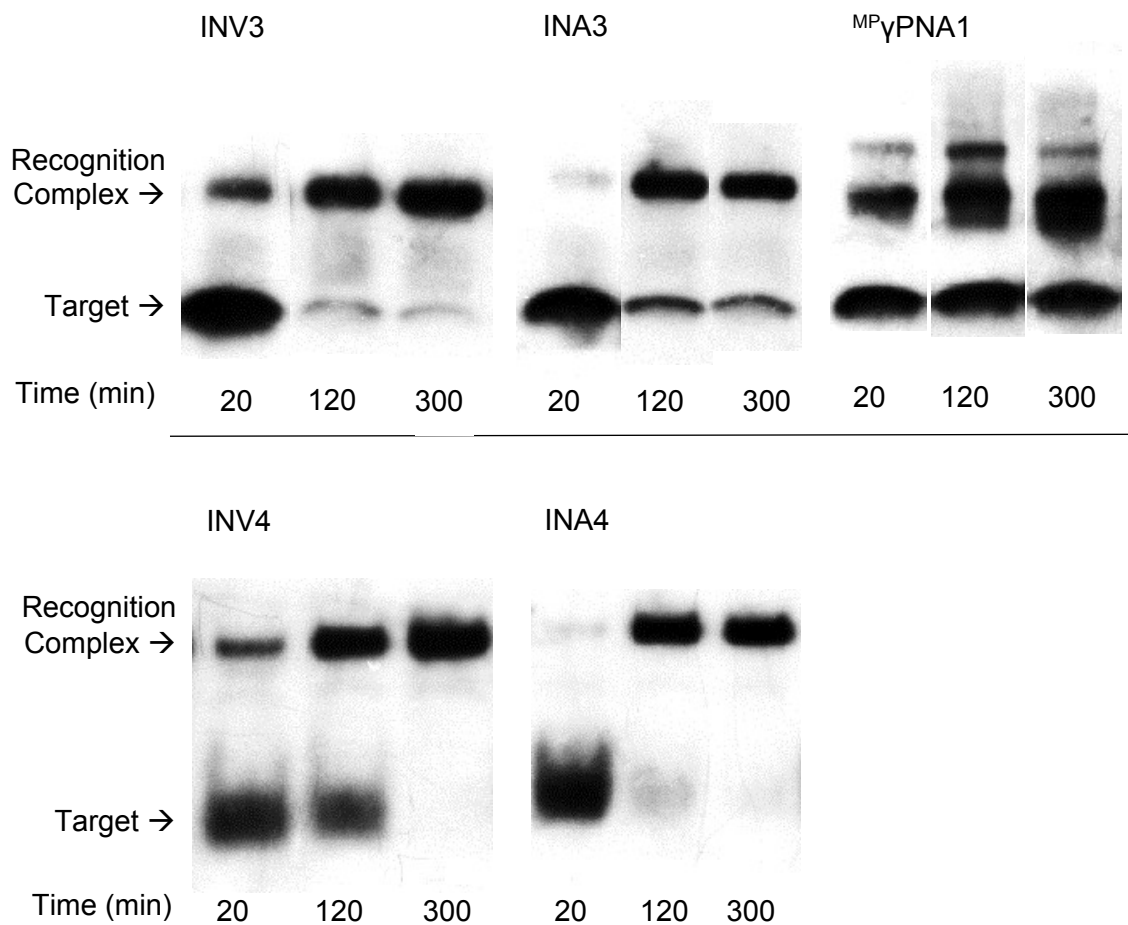
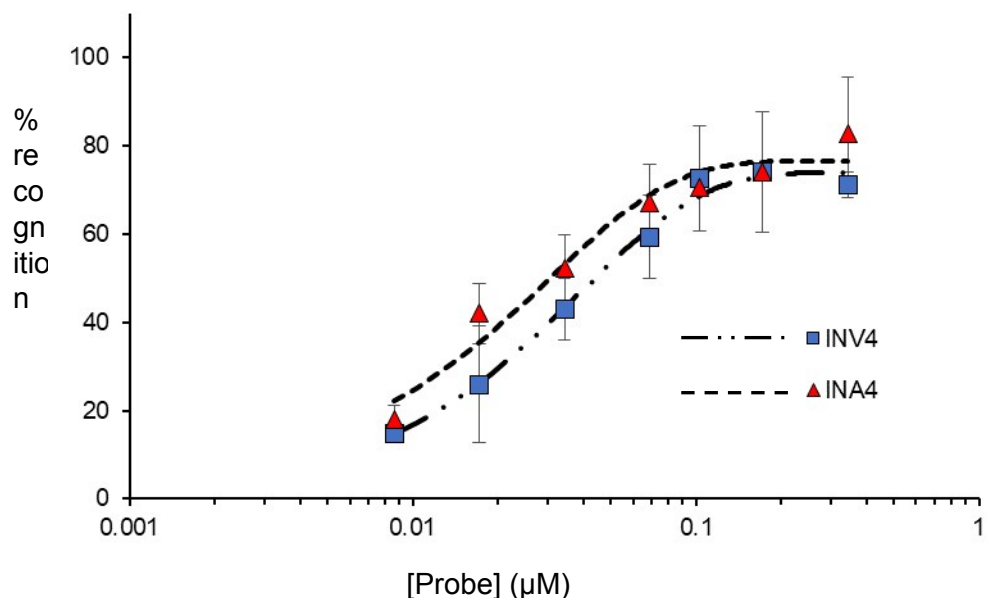


Figure S14. Representative electrophoretograms from time-course experiments using Invader, INA and $^{MP}\gamma$ PNA1 probes (composite images). A 5-fold molar probe excess was incubated with **DH1** (34.4 nM) for the indicated time at 37 °C. For additional details regarding experimental conditions, see Figure S8. For time-course curves, see Figures 5 and S15.

a)



b)

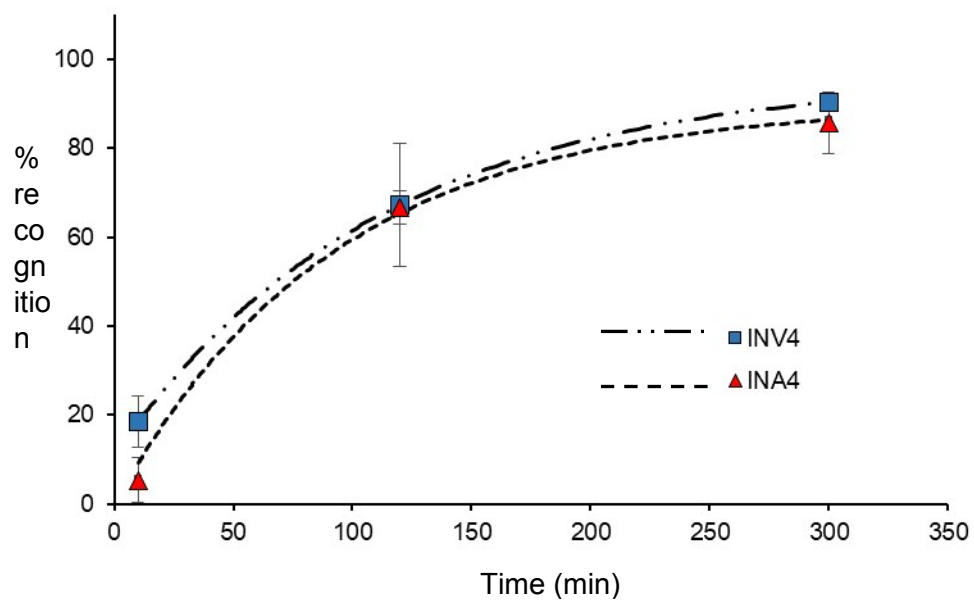


Figure S15. a) Dose-response curves for **INV4** and **INA4** incubated with **DH1** at 37 °C for 2.5 hours. b) Time-course curve for **INV4** and **INA4** incubated with **DH1** at 5-fold molar excess at 37 °C. For additional details regarding experimental conditions, see Figure S8.

Table S10. Sequences and T_m values of DNA hairpins used in this study.^a

DH	Sequence	T_m (°C)
1		58.5
2		60.5
3		63.5
4		63.0
5		60.0
6		62.5
7		62.5

^aFor experimental conditions, see Table 1. Table previously published in reference 1.

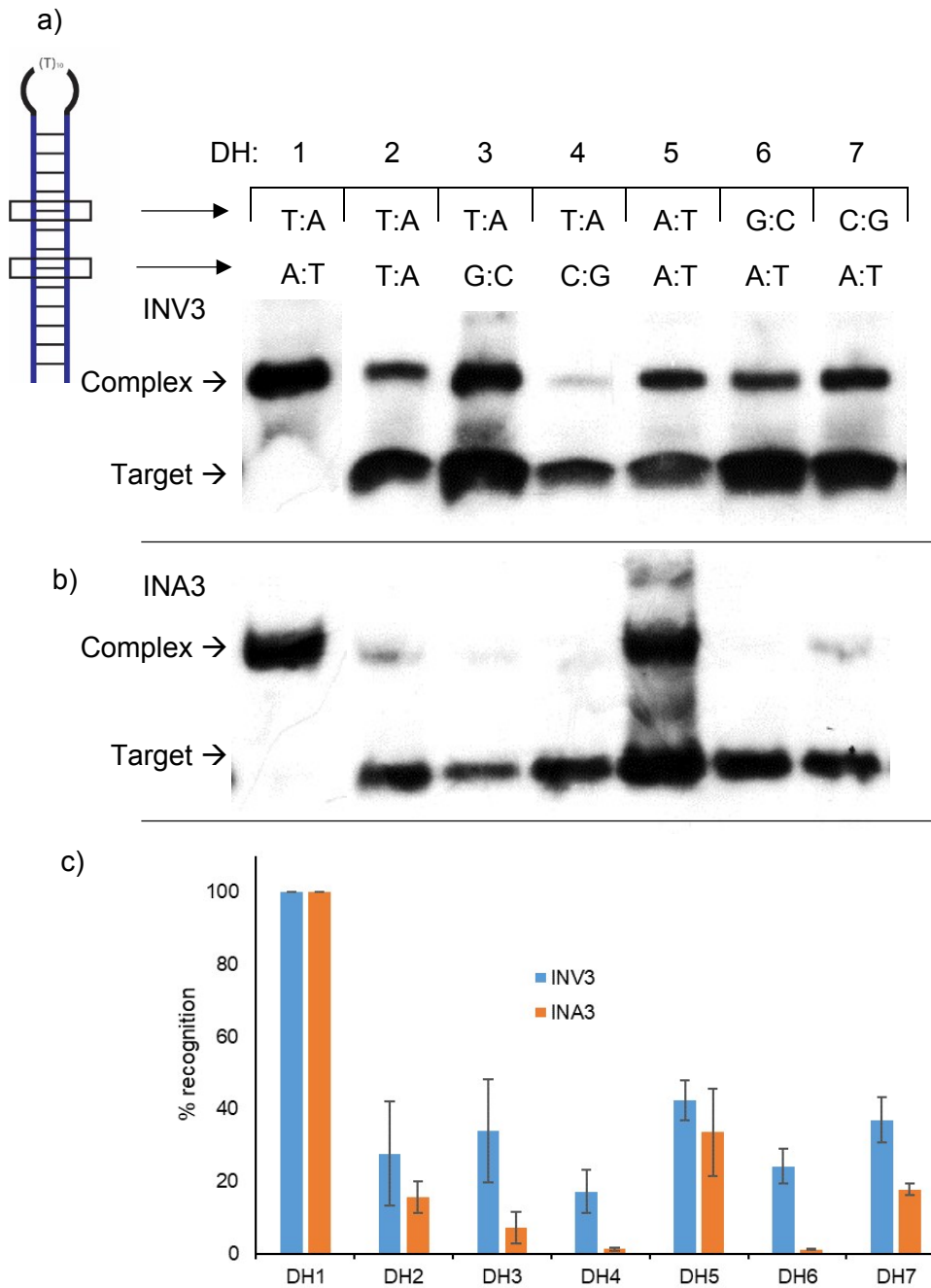


Figure S16. Binding specificity of **INV3** and **INA3** when used at a very high excess. Representative electrophoretograms from experiments in which a 75-fold molar excess of **INV3** (a) or **INA3** (b) were incubated with **DH1-DH7** (34.4 nM) at 37 °C for 2.5 h. (c) Histograms depict averaged results from at least three separate experiments. Error bars represent standard deviation. Experimental conditions are as described in Figure S8.

Supporting references

- S1) D. C. Guenther, G. H. Anderson, S. Karmakar, B. A. Anderson, B. A. Didion, W. Guo, J. P. Verstegen and P. J. Hrdlicka, *Chem. Sci.*, 2015, **6**, 5006-5015.
- S2) J.-L. Mergny and L. Lacroix, *Oligonucleotides*, 2003, **13**, 515-537.
- S3) D. M. Crothers, *Biopolymers*, 1968, **6**, 575-584.
- S4) S. C. Jain, C. Tsai and H. M. Sobell, *J. Mol. Biol.*, 1977, **114**, 317-331.